30th ITS World Congress, Dubai, UAE, 16-20 September 2024

Paper ID #230

The effects of latency on teleoperated driving maneuvers

Xunbi A. Ji[1*], Sergei S. Avedisov[2], Mohammad Irfan Khan[2], Onur Altintas[2], Gábor Orosz[1,3]

1. Department of Mechanical Engineering, University of Michigan, MI 48109, USA ([*]xunbij@umich.edu)

2. Toyota Motor North America R&D – InfoTech Labs, Mountain View, CA 94043, USA

3. Department of Civil and Environmental Engineering, University of Michigan, MI 48109, USA

Abstract

We investigate the effects of latencies on performance of teleoperated driving. A dimensionless vehicle dynamics model with a scaled delay is analyzed to reduce the number of parameters. We study the control performance through stability analysis, i.e., whether the vehicle converges to a given path and the convergence speed. We demonstrate that the velocity, the time delay in the control loop and the path curvature all affect performance. Furthermore, increasing the product of the velocity and overall time delay degrades the performance and the vehicle may fail to follow the reference path. Selecting control gains based on the fastest convergence rate provides sufficient robustness against delay and velocity changes and the stability analysis can be extended to scenarios with curved paths. Numerical simulations of the vehicle following curved paths in a realistic parking scenario based on real-life measurements are provided to demonstrate the negative effects of large curvature on performance.

Keywords:

Communication latency, teleoperated driving, stability analysis, numerical simulations

1. Introduction

Alongside the rise of automated driving [1], where vehicles control their motion using on-board computation units; remote driving, where control commands are given through a communication network, is also rising a supplement to automated driving [2, 3]. The architecture of a remote driving control loop is shown in Fig. 1(a). The controller on the remote end can be either an experienced human operator or an intelligent algorithm running in the remote center. The status of the vehicle and the surrounding environment are sent to the remote controller via the uplink part of the network. The control commands are sent back to the vehicle via the downlink part of the network and then executed by the vehicle's actuators. One of the biggest challenges introduced by such a communication structure is latency (also called time delay) [4].

Such latency originates from multiple sources:

1. Time needed to encode, send, receive and decode data packets.

2. Loss of data packets due to the network traffic.
3. Processing time of the remote operator.
4. Actuation delay of the vehicle.

While researchers and engineers have been working on designing low-latency communication networks and reducing latency in video streaming [5, 6] to address the problem caused by the first three latency sources, the overall latency cannot be eliminated. For example, an automated vehicle with internal combustion engine can have an actuation delay in the longitudinal dynamics around 0.6 seconds which is not negligible [7]. The overall latency in the control loop also varies stochastically in time, due to the stochasticity of packet loss in the communication network [8, 9], while the average latency may be estimated for given network conditions and the effect of stochasticity may be neglected when the packet loss ratio is low. It is crucial to account for the latency when evaluating the controller's performance [10]. In this work, we approximate the stochastic time-varying latency by a constant value and perform the analysis and simulations accordingly.

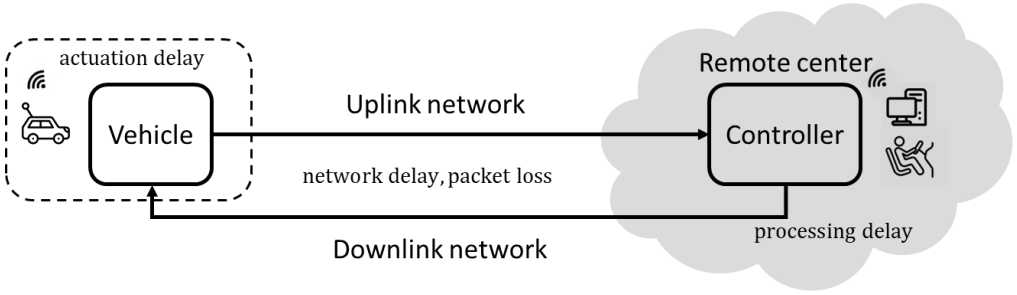

Figure 1 - Block diagram for the teleoperated driving system

The rest of this paper is organized as follows. In Section 2, we first introduce the vehicle model and the steering controller with delay when following a straight path. Then we reduce the number of parameters by nondimensionalization and linearize the dimensionless model to perform stability analysis. We analytically obtain stability boundaries and the control gains corresponding to the fastest convergence rate. The robustness of the fastest-convergence gains against the change of delay and velocity in the system is investigated. In Section 3, we present numerical simulations to illustrate the effect of path curvature on the path following stability. Lastly, we conclude the results in Section 4 and provide insights for future study.

2. Vehicle models and steering controller for following a straight path

2.1 Bicycle model with rigid wheels

In this paper, we use a bicycle model [11] with rigid wheels to represent the teleoperated vehicle as illustrated in Fig. 2 (a). This bicycle model provides high enough fidelity which captures most of the daily-driving maneuvers and also simplifies the analysis significantly. That is, the rear axle is simplified to a single wheel and the front wheels are also merged as a single wheel. The center point R of the vehicle's rear axle has the coordinates $(x_{\mathrm{R}}, y_{\mathrm{R}})$ while the yaw angle ψ describes the orientation of the vehicle. The longitudinal velocity v at point R aligns with the symmetry axis of the vehicle according to the rigid wheel assumption and the steering angle γ is assigned by the controller. The wheelbase is denoted by l. Thus, the model [12] can be expressed by the delay differential equations

$$\frac{\mathrm{d}x_\mathrm{R}}{\mathrm{d}t}(t) = v\cos\psi(t),$$
$$\frac{\mathrm{d}y_\mathrm{R}}{\mathrm{d}t}(t) = v\sin\psi(t), \qquad (1)$$
$$\frac{\mathrm{d}\psi}{\mathrm{d}t}(t) = \frac{v}{l}\tan\gamma(t-\tau),$$

where τ denotes the overall latency in the teleoperated system (Fig. 1). Initially we consider the control goal to be following the straight path $y = 0, \psi = 0$ (Fig 2(c)). To achieve this, we consider the controller $\gamma = \arctan(-k_\psi\psi - k_y y_\mathrm{R})$, see [13,14] for similar applications. Thus, for a given initial position and yaw angle, one can obtain the trajectory of the point R and orientation of the vehicle as a function of time by integrating (1). The lateral position y_R is plotted as a function of time in Fig. 2(b) for different velocities v and delays τ, such that the scaled product $\frac{v\tau}{l}$ is kept constant; see Scenario A and B in Table 1. The corresponding trajectories of point R are visualized in the (x, y) plane in panel (c) and the two simulations give the same trajectory. That is, increasing the velocity of vehicle has the same effect on the trajectory as increasing the delay in the system. This motivates the nondimensionalization of the system to reduce the number of parameters for stability analysis in the next section.

Scenario	Speed (v)	Delay (τ)	Scaled delay $\left(\hat{\tau} = \frac{v\tau}{l}\right)$
A	2.73 [m/s]	0.4 [s]	0.4
B	5.46 [m/s]	0.2 [s]	

Table 1 - Parameters for scenario A and B shown in Figure 2, such that speeds and delays are different but the scaled delay is the same. The same wheelbase $l = 2.73$ [m] is used for both scenarios.

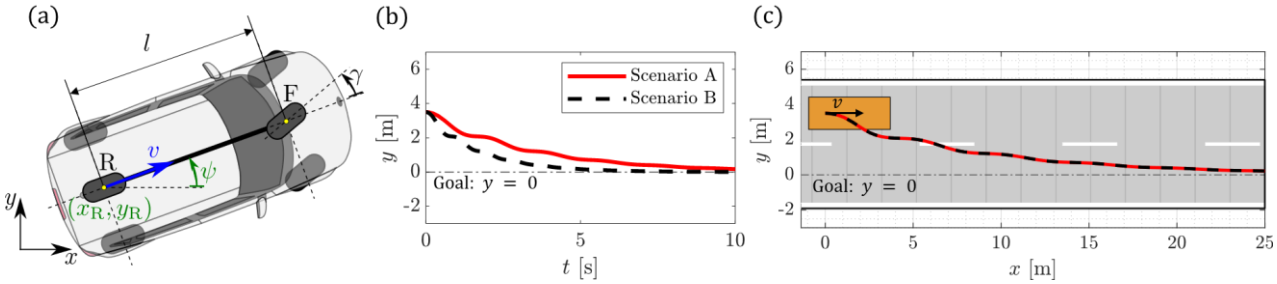

Figure 2 – (a) Bicycle model with steering control. (b) Lateral position of the vehicle as a function of time for simulated scenarios A and B (Table 1). (c) Trajectories of the vehicle for the same simulations. The simulations are based on system (1).

2.2 Nondimensionalization and linearization

We rescale the time and space in system (1) using $\hat{t} = \frac{v}{l}t$, $\hat{\tau} = \frac{v}{l}\tau$, $\hat{x}_\mathrm{R} = \frac{x_\mathrm{R}}{l}$, $\hat{y}_\mathrm{R} = \frac{y_\mathrm{R}}{l}$ which results in system (2), and then linearize system (2) around the straight running motion $\hat{x}_\mathrm{R}^* = \hat{t}, \hat{y}_\mathrm{R}^* = 0, \psi^* = 0$ to obtain system (3):

$$\text{System (1)} \xrightarrow{\text{rescale}} \begin{cases} \frac{\mathrm{d}\hat{x}_\mathrm{R}}{\mathrm{d}\hat{t}} = \cos\psi(\hat{t}), \\ \frac{\mathrm{d}\hat{y}_\mathrm{R}}{\mathrm{d}\hat{t}} = \sin\psi(\hat{t}), \\ \frac{\mathrm{d}\psi}{\mathrm{d}\hat{t}} = -k_\psi\psi(\hat{t}-\hat{\tau}) - k_y l\hat{y}_\mathrm{R}(\hat{t}-\hat{\tau}). \end{cases} \quad (2) \xrightarrow{\text{linearize}} \begin{cases} \frac{\mathrm{d}\tilde{x}}{\mathrm{d}\hat{t}} = 0, \\ \frac{\mathrm{d}\tilde{y}}{\mathrm{d}\hat{t}} = \tilde{\psi}, \\ \frac{\mathrm{d}\tilde{\psi}}{\mathrm{d}\hat{t}} = -k_\psi\tilde{\psi}(\hat{t}-\hat{\tau}) - k_y l\tilde{y}(\hat{t}-\hat{\tau}), \end{cases} \quad (3)$$

where we define $\tilde{x} = \hat{x}_\mathrm{R} - \hat{x}_\mathrm{R}^*$, $\tilde{y} = \hat{y}_\mathrm{R} - \hat{y}_\mathrm{R}^*$, $\tilde{\psi} = \psi - \psi^*$. Notice that the first equation in (3) is decoupled from the second and third equation, i.e., the stability of the lateral dynamics only depends on the second and third rows. We can rewrite the last two delay differential equations into the matrix form

$$\begin{bmatrix} \frac{\mathrm{d}\tilde{y}}{\mathrm{d}\hat{t}}(\hat{t}) \\ \frac{\mathrm{d}\tilde{\psi}}{\mathrm{d}\hat{t}}(\hat{t}) \end{bmatrix} = \mathbf{A}\begin{bmatrix} \tilde{y}(\hat{t}) \\ \tilde{\psi}(\hat{t}) \end{bmatrix} + \mathbf{B}\begin{bmatrix} \tilde{y}(\hat{t}-\hat{\tau}) \\ \tilde{\psi}(\hat{t}-\hat{\tau}) \end{bmatrix}, \quad \text{with } \mathbf{A} = \begin{bmatrix} 0 & 1 \\ 0 & 0 \end{bmatrix}, \mathbf{B} = \begin{bmatrix} 0 & 0 \\ -k_y l & -k_\psi \end{bmatrix}. \quad (4)$$

In this dimensionless linear system, the velocity only appears in the scaled delay $\hat{\tau} = \frac{v\tau}{l}$. This implies that the velocity has the exact same effect on stability as the original delay τ and explains the overlap of the trajectories in Fig. 2(c) where the product $v\tau$ is the same in both scenarios.

2.3 Linear stability analysis and the fastest-convergence gain

The characteristic equation for system (4) is given by $\det\left(\lambda\mathbf{I} - \mathbf{A} - \mathbf{B}e^{-\lambda\hat{\tau}}\right) = 0$ and the stability boundary can be obtained by substituting the roots $\lambda = \mathrm{j}\omega$ $(\omega \geq 0)$ and solving for $k_y l$ and k_ψ. This leads to the stability boundaries $k_\psi = \omega\sin(\omega\hat{\tau}), k_y l = \omega^2\cos(\omega\hat{\tau}), \omega > 0$ and $k_y l = 0$which are shown for the scaled delay value $\hat{\tau} = 0.4$ in the $(k_\psi, k_y l)$ plane as shown in Fig. 3 (b). The region enclosed by these two boundaries is the stable region. If the control gains are selected from the stable region, the vehicle converges to the straight path $y = 0$. Still, when different control gains selected from the stable domain the control performance may vary significantly. These differ in how fast the vehicle converges to the straight path. Simulations of the system (1) with different gains are shown in Fig. 3 (b). Although all three gains are selected from the stable region in Fig. 3 (a), they result in significantly different behaviors in terms of convergence.

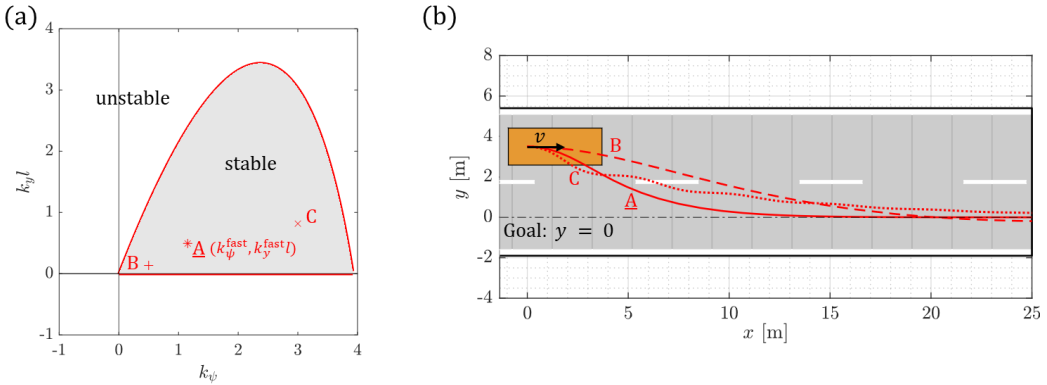

Figure 3 – (a) Stability chart for $\hat{\tau} = 0.4$; the shaded area indicates the stable region. Three sets of gains are marked as these are used in simulations to compare the control performance. The star indicates the gains with the fastest convergence rate. (b) Simulations of the lane change with different control gains corresponding to (a). The simulations are based on the system (3).

One may substitute the roots $\lambda = \rho + j\omega$ $(\omega \geq 0)$ into the characteristic equation to obtain the performance contours for different ρ values. For $\rho < 0$, the dimensionless system is stable and the vehicle converges to the straight path exponentially with rate ρ. The smaller the ρ is, the faster the system converges to $y = 0$. The closed form expression for the fastest convergence rate (smallest possible ρ) and the corresponding control gains can be derived analytically as

$$\begin{aligned} \rho_{\text{fast}} &= \frac{\sqrt{2}-2}{\hat{\tau}}, \\ k_{\psi}^{\text{fast}} &= -\frac{a}{\hat{\tau}}, \\ k_{y}^{\text{fast}} l &= \frac{b}{\hat{\tau}^2}, \end{aligned} \tag{5}$$

where $a = -e^{\sqrt{2}-2}(2-2\sqrt{2})$ and $b = e^{\sqrt{2}-2}(10\sqrt{2}-14)$. Observe that the formulae in (5) only depend on the scaled delay $\hat{\tau}$. The control gains with the fastest convergence rate (for $\hat{\tau} = 0.4$) are indicated by a red star in Fig. 3(a). Fig. 3(b) visualizes the corresponding trajectories when the vehicle is doing a lane change with different control gains selected from the stable region. The fastest-convergence gains (case A) indeed make the system converge to the desired path quickly without any oscillation.

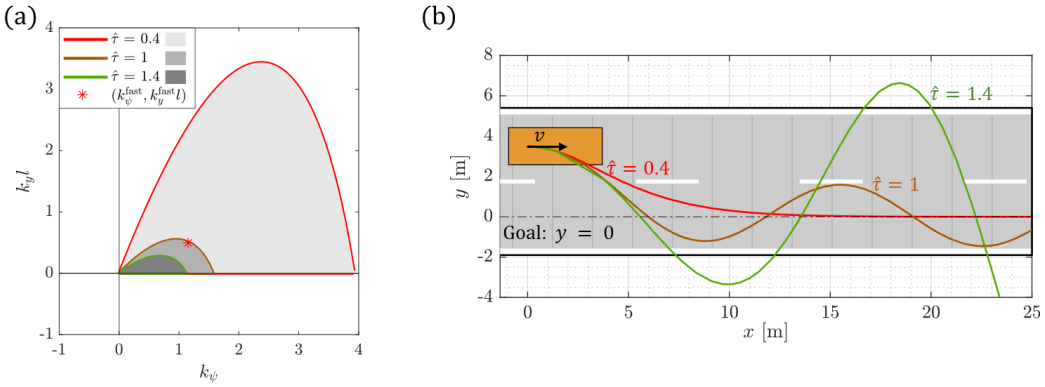

Figure 4 – (a) Stability boundaries for different $\hat{\tau}$ values. Note: the set of fastest-convergence gains for $\hat{\tau} = 0.4$ is located near the boundary of $\hat{\tau} = 1$. (b) Simulations of a lane change maneuver using the fastest-convergence gains from Fig. 3(a), while using different $\hat{\tau}$ values. The simulations are based on the system (3).

When the scaled delay increases, the stable region shrinks as in Fig. 4(a). The previously chosen gain combination for $\hat{\tau} = 0.4$ can lead to oscillatory or diverging trajectory if it is located too close to the new stability boundary or outside the stable region for larger delays. For example, the brown stability boundaries for $\hat{\tau} = 1$ still enclose the fastest-convergence gains for $\hat{\tau} = 0.4$ but the same gain now leads to significant oscillations as shown by the brown trajectory in Fig. 4(b). If we further increase the scaled delay to $\hat{\tau} = 1.4$, the corresponding green stability boundaries no longer enclose the selected gain combination, resulting an unstable trajectory (green) in the panel (b). Fig. 4 illustrates that the fastest-convergence gain combination selected for a given $\hat{\tau}$ is at the stability boundary for a larger critical delay $\hat{\tau}_{\text{cr}}$. The relationship between the critical delay $\hat{\tau}_{\text{cr}}$ and $\hat{\tau}$ is given by

$$\hat{\tau}_{\text{cr}} = \frac{\sin^{-1}\left(\frac{a}{c}\right)}{c}\,\hat{\tau} \quad \xrightarrow{c=\sqrt{\frac{a^2+\sqrt{a^4+4b^2}}{2}}} \quad \hat{\tau}_{\text{cr}} \approx 2.52\,\hat{\tau}, \tag{6}$$

which is linear and does not depend on any parameter. This relationship also implies that if the fastest-convergence gain combination is selected for a certain latency and driving velocity, the system will still be stable even when the latency or the velocity increases up to 2.5 times of its original value.

3. Teleoperated driving on a curved path

In this section, we study the remote driving task using numerical simulations when the vehicle aims to follow a curved path [13], and we investigate the effect of curvature of the reference path on the steering performance. We consider the case where the remote controller needs to move the vehicle from a starting position on the right to a finishing position on the left within the parking lot, as shown in Fig. 5(a) and (b). Different paths are planned for different destinations. The desired curvature and the desired velocity along the paths can be expressed as functions of the path arclength. Fig. 5(c) and (d) define the different references paths A and B shown in (a) and (b), with maximum curvatures 0.0125 m^{-1} and 0.1245 m^{-1}, respectively. The vehicle first accelerates from a standstill to the maximum velocity of 4 m/s, then coasts at this velocity in the middle segment and finally decelerates to a full stop at the end. Fig. 5(e) and (f) depict the numerical simulation results of the vehicle following reference path A (dashed magenta line) and reference path B (dashed black line) with same control gains, same overall latency $\tau = 0.341$ second and similar velocity plans. The trajectory of point R on the vehicle is plotted as a blue solid curve for each scenario and the area covered by the vehicle along the trajectory (swept volume) is covered by orange rectangles at discretized time moments. The vehicle can follow path A and park straight into the closest spot on the other side without noticeable deviations from the designed path. However, it fails to deliver the same performance along path B and violates the parking spot boundaries. Indeed, the control performance degenerates as the curvature increases.

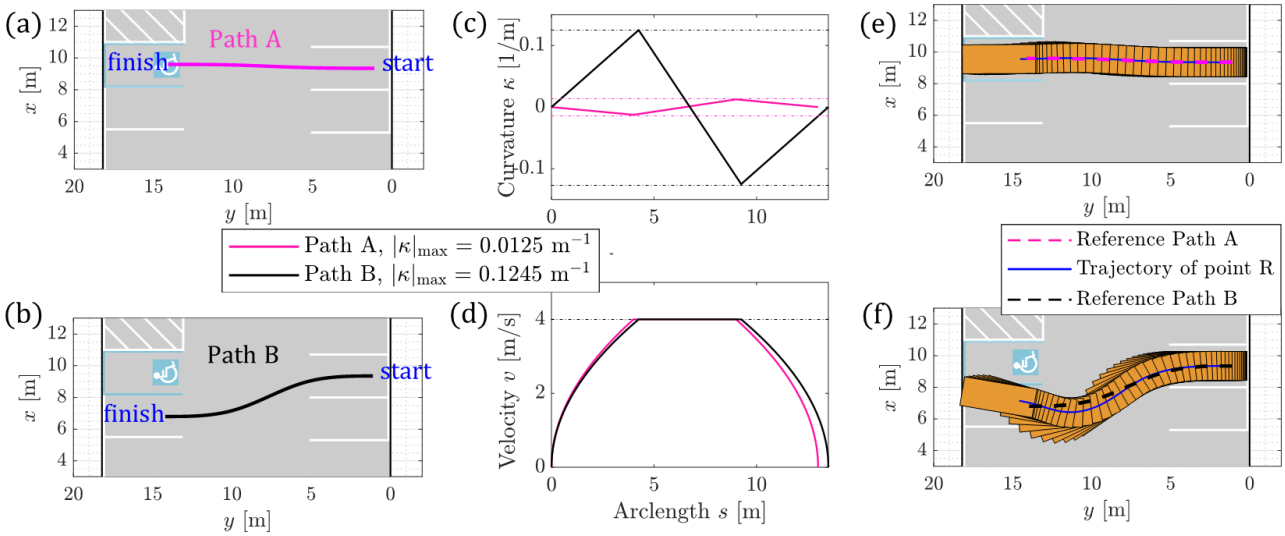

Figure 5 – (a-b) The desired paths A and B for moving the vehicle from the start to different finish positions (c) The desired curvature along the reference paths. (d) The desired velocity along the reference paths. (e-f) Simulations of the vehicle following paths A and B. Reference paths are the same as paths in (a-d), but indicated in dashed lines for better visibility.

4. Conclusion

In this paper, we demonstrated the effect of network latency on teleoperated driving. We studied the performance of given controllers analytically and numerically for the case of following a straight path and presented numerical simulations for the case of following a curved path. We showed that there are three key factors which affect the linear stability and the control performance for any state feedback controllers: the overall latency in the control loop, the longitudinal velocity of the vehicle, and the curvature of the path. The velocity of the vehicle has the same effect on the stability as the latency while considering paths with larger curvature can also make the system less stable when following the path. The presented analytical and numerical methods help in evaluating controllers with latency, and further facilitate the motion planning unit to make better decisions. If the controller is designed for a nominal delay with desired performance, but the actual overall latency in the loop doubles, the motion planner can simply half the suggested velocity to ensure the stability and similar performance. Moreover, the motion planner can suggest a path with less curvature to have higher tolerance to increases in latency. In the future, nonlinear stability analysis will be employed and more complex vehicle models will be considered for high velocity scenarios.

References

1. Ersal, T., I. Kolmanovsky, N. Masoud, N. Ozay, J. Scruggs, R. Vasudevan, G. Orosz (2020). Connected and automated road vehicles: state of the art and future challenges. *Vehicle System Dynamics*, 58(5), pp. 672-704.
2. Kang, L., W. Zhao, B. Qi, S. Banerjee (2018). Augmenting self-driving with remote control: Challenges and directions. In *19th International Workshop on Mobile Computing Systems & Applications*, pp. 19-24.
3. Liu, R., D. Kwak, S. Devarakonda, K. Bekris, L. Iftode (2017). Investigating remote driving over the LTE network. In *9th International Conference on Automotive User Interfaces and Interactive Vehicular Applications*, pp. 264-269.
4. Neumeier, S., P. Wintersberger, A.K. Frison, A. Becher, C. Facchi, A. Riener (2019). Teleoperation: The holy grail to solve problems of automated driving? Sure, but latency matters. In *11th International Conference on Automotive User Interfaces and Interactive Vehicular Applications*, pp. 186-197.
5. Yu, Y., S. Lee (2022). Remote driving control with real-time video streaming over wireless networks: Design and evaluation. *IEEE Access*, 10, pp. 64920-64932.
6. El Marai, O., T. Taleb (2020). Smooth and low latency video streaming for autonomous cars during handover. *IEEE Network*, 34(6), pp. 302-309.
7. Ji, X.A., T.G. Molnár, A.A Gorodetsky, G. Orosz, (2021). Bayesian inference for time delay systems with application to connected automated vehicles. In *2021 IEEE International Intelligent Transportation Systems Conference (ITSC)*, pp. 3259-3264.
8. Lucas-Estañ, M. C., B. Coll-Perales, M. I. Khan, S. S. Avedisov, O. Altintas, J. Gozalvez, M. Sepulcre (2023). Support of Teleoperated Driving with 5G Networks. In *98th IEEE Vehicular Technology Conference*

(VTC2023-Fall)

9. Qin, W. B., G. Orosz (2017). Scalable stability analysis on large connected vehicle systems subject to stochastic communication delays. *Transportation Research Part C*, 83, pp. 39-60.
10. Ghorai, P., A. Eskandarian, Y.K. Kim (2020). Study the effect of communication delay for perception and collision avoidance in cooperative autonomous driving. *American Society of Mechanical Engineers International Mechanical Engineering Congress and Exposition*, 84553, pp. V07BT07A015.
11. Rajamani, R (2011). Vehicle dynamics and control. *Springer Science & Business Media*.
12. Qin, W.B., Y. Zhang, D. Takács, G. Stépán, G. Orosz (2022). Nonholonomic dynamics and control of road vehicles: moving toward automation. *Nonlinear Dynamics*, 110(3), pp. 1959-2004.
13. Beregi, S., S.S. Avedisov, C.R. He, D. Takács, G. Orosz (2023). Connectivity-based delay-tolerant control of automated vehicles: theory and experiments. *IEEE Transactions on Intelligent Vehicles*, 8(1), pp. 275-289.
14. Vörös, I., G. Orosz, D. Takács (2023). On the global dynamics of path-following control of automated passenger vehicles. *Nonlinear Dynamics*, 111(9), pp. 8235-8252.